RSC Advances

Synthesis and characterization of novel thin film nanocomposite reverse osmosis membranes with improved organic fouling properties for water desalination

Journal:	*RSC Advances*
Manuscript ID:	RA-ART-12-2014-016177.R2
Article Type:	Paper
Date Submitted by the Author:	04-Feb-2015
Complete List of Authors:	Ghanbari, Mohammad; Universiti Teknologi Malaysia, Emadzadeh, Daryoush; Universiti Teknologi Malaysia, Lau, woeijye; Universiti Teknologi Malaysia, Matsuura, Takeshi; University of Ottawa, Ismail, A.F.; Universiti Teknologi Malaysia (UTM), Advanced Membrane Technology Center

Synthesis and characterization of novel thin film nanocomposite reverse osmosis membranes with improved organic fouling properties for water desalination

M. Ghanbari[a], D.Emadzadeh[a,b], W.J. Lau[a], T. Matsuura[a,c], A.F.Ismail[a*]
[a]Advanced Membrane Technology Research Centre (AMTEC), Universiti Teknologi Malaysia, 81310 Skudai, Johor, Malaysia
[b]Department of Chemical Engineering, Gachsaran Branch, Islamic Azad University, Gachsaran, Iran
[c]Industrial Membrane Research Laboratory, Department of Chemical and Biological Engineering, University of Ottawa, 161 Louis Pasteur St, Ottawa, Canada ON K1N 6N5
*Corresponding author: Email address: *afauzi@utm.my*
Tel.: +60 7 553 5592; fax: +60 7 558 1463.

Abstract

In this study, a new type of thin film nanocomposite (TFN) reverse osmosis (RO) membranes wasprepared by incorporating different amounts of halloysite nanotubes (HNTs)into the polyamide (PA) selective layer via in-situ interfacial polymerization. The effect of HNTs incorporation into the PA selective layer on the surface morphology, separation performance and antifouling properties of the membranes were thoroughly investigated and discussed. The presence of HNTs in PA layer was verified using EDX, XRD and FTIR analysis. The "leaf-like" outgrowth morphology of PA layer was observed using FESEM. Upon addition of HNTs, the hydrophilicity, surface roughness and water flux of TFN membranes have all increased. The water flux enhancement can be ascribed to higher hydrophilicity and additional water pathways through porous HNTs in TFN membranes. It is noteworthy that the TFN membrane that was embedded with 0.05 wt./v% HNTs (labeled as TFN0.05) could exhibit water flux as high as 36 L/m^2.h (at 15 bar gauge) with NaCl rejection maintained at 95.6%. In comparison to the control thin film composite (TFC) membrane, the water flux of TFN0.05 membrane was 90% higher. Although further increase in HNTs loading to 0.1 wt./v% could result in greater water flux, its RO performance was compromised by a significant decrease in NaCl rejection. Besides offering greater water flux, theTFN0.05 membrane also showed better antifouling affinity than HNTs-free TFC membrane. It is most probably due to the increase in hydrophilicity as well as surface negative charge upon addition of HNTs. Based on the results obtained in this work, it can be concluded that incorporating an appropriate amount of HNTs into PA rejection layer could potentially improve the performance of TFC membrane during RO applications.

Keywords: thin film nanocomposite membrane; reverse osmosis; halloysite nanotube; antifouling; water treatment.

Highlights:

- Incorporation of HNTs into PA layer altered the structural and separation characteristics of composite membrane
- Synthesized TFN RO membrane displayed greater water flux without compensating NaCl rejection.
- Embedding HNTs into PA layer improved fouling resistance of TFN membrane.

1. Introduction

Scarcity of fresh water caused by social, economic, and technological developments has become a major concern for many countries. In order to address this issue, it is necessary to identify novel, cheap, and energy efficient wastewater treatment techniques that pose no threat to environment or human health[1]. Of the many treatment methods available, membrane technology, in particular, reverse osmosis (RO) has attracted the most extensive attention for drinkable water production. RO membrane is estimated to be used in more than 50% of the operating desalination vessels globally [2]. The popularity of RO membrane can be ascribed to low cost, low energy consumption, short construction cycle, simple equipment and operation, as well as simplicity of control [1].

The modern desalination industry requires treatment methods with high productivity. Benefiting from unique features of thin film composite (TFC) polyamide (PA) membranes[3, 4], RO desalination has successfully fulfilled this criterion owning to its low hydraulic resistance[2, 5].However, one can realize that various strategies have been proposed and investigated with the aims of further improving the permeability of TFC PA membranes. These include membrane post treatment [6, 7], surface functionalization[8, 9], synthesizing of PA layer of different chemistries [10, 11], and so on. It must be noted that besides improving membrane water permeability, these approaches in certain case could improve membrane antifouling resistance. Due to the increasing demands of desalination membranes with improved permeate flux/salt rejection and higher fouling performance, continuous researches and innovations in RO membranes are still necessary[12, 13].

The fact that the top PA layer of TFC membrane is prone to fouling is the main obstacle of this membrane to be sustainably used in RO applications. The fouling in general is caused by the deposition of colloidal and particulate matter (colloidal fouling), organic macromolecules (organic fouling), sparsely soluble inorganic compounds (inorganic fouling or scaling) and microorganisms (biofouling) on the membranes[14]. This fouling increases the process energy consumption and shortens membrane lifetime by decreasing the quality and quantity of the permeate [15, 16]. Several approaches have been recommended to improve the fouling resistance of PA layer of TFC RO membranes which include selection of new monomers, improvement of fabrication process, surface modification of PA selective layer by either physical or chemical methods and the development of hybrid organic/inorganic TFC RO membrane [17].

Of these approaches, developing RO membrane with nanomaterials embedded within the thin PA selective layer has attracted significant focus from membrane scientists, owing to the unique characteristics of nanomaterials to match with the thickness of PA layer. This new generation of composite membrane is generally named as thin film nanocomposite (TFN) membranes as inorganic nanomaterials are introduced to organic PA film of TFC membrane during interfacial polymerization process [18].

In this work, we will explore the potential of using alumina-silicates as inorganic nanomaterials in the synthesis of novel TFN membranes for RO application. Alumina-silicates with chemical composition of $Al_2Si_2O_5(OH)_4{\cdot}2H_2O$ are generally known as halloysite nanotubes (HNTs). Since HNTs are harvested from natural and biocompatible sources, they are economically attainable and have environmentally friendly features which make them suitable for membrane preparation[19, 20].While the outer layer of HNTs is negatively charged due to the presence of siloxane groups (Si-O-Si), numerous hydroxyl groups(Al-OH) in the internal tube wall make the inner layer positively charged [20, 21].This unique structure guarantees HNTs for applications in water treatment [22]. Moreover, specific features of HNTs such as their unique crystal structure, tubular form, and low density of hydroxyl functional groups enable them to be dispersed easily in a polymer matrix [23-25]. Compared to carbon nanotubes (CNTs),these natural materials possess various outside and inside chemical properties, contain adequate hydroxyl groups on the surface, and are more cost effective[26, 27]. It is worth noting that CNTs and HNTs have similar tubular structure and both bear hydrophilic groups.

Some studies have focused on application of HNTs in improving fouling behaviour of mixed matrix membrane for ultrafiltration process[19, 24, 28, 29].But, approach on using HNTs in preparing TFN membranes for RO applications have not yet to be reported. In this work, hydrophilic HNTs are used to fabricate TFN membranes for low pressure RO application and these membranes are prepared via interfacial polymerization process by adding HNTs into the organic phase. Characterization of control TFC and TFN membranes and evaluation of membrane performance in terms of water flux, salt rejection and fouling resistance will be performed and discussed in detail.

2. Experimental

2.1 Materials

Polysulfone (PSf) Udel P-3500 in pellet form (Solvay Advanced Polymers), dimethylacetamide (DMAC, >99.5%, Merck), polyvinylpyrrolidone (PVP K30, Sigma-Aldrich), bovine serum albumin (BSA, 66 kDa, Sigma-Aldrich) and sodium chloride (NaCl, >99.5%, Merck) were used as solvent, additive, foulant and salt, respectively. Halloysite nanotubes (HNTs) with inner tube diameter of 5-15 nm was purchased from Sigma Aldrich. Synthesis of PA selective layer for TFC and TFN membranes was carried out using 1,3-phenylenediamine (MPD, >99%, Merck) and 1,3,5-benzenetricarbonyl trichloride (TMC, >98%, Merck) as amine and acyl chloride monomer, respectively.

2.2. Flat sheet TFN RO membranes

2.2.1. Preparation of substrate

A dope solution containing 17.5% PSf, 0.5% PVP and 82% DMAC was used for preparing substrate of TFN RO membrane. Trapped air bubbles inside the prepared dope solution were removed by leaving the solution in an ultrasonic bath at 25^{o}C for 2 h. After casting the prepared solution on a glass plate with a casting knife, the cast film was submerged into a water coagulation bath at room temperature. After the membrane was peeled off from the glass plate spontaneously, it was immersed into another water bath for 24 h to remove residual solvent, which was followed by storage in DI water.

2.2.2. Preparation of polyamide selective layer

Interfacial polymerization on the surface of a pre-cast PSf substrate resulted in formation of the top PA active layer on the supporting membrane. Cyclohexane was used as the organic solvent for this study as it could provide better dispersion for HNTs compared to n-hexane. The chance of nanoparticles agglomeration was reduced by sonicating the mixture for 3 h. Interfacial polymerization process was initiated by pouring 100 mL of 2% (w/v) MPD aqueous solution to the surface of the PSf substrate. To assure penetration of MPD solution into the pores of the substrate, it was held horizontally for 2 min. The excess MPD solution was drained off and its residual droplets on the substrate surface were removed using a soft rubber roller. Then, 100 mL of 0.1% (w/v) TMC solutions in cyclohexane containing various quantities of HNTs (0.01, 0.05 and 0.1 w/v%) were added to the substrate that was contacted with MPD solution. After 1 min contact with the surface, the TMC solution was drained off. The unreacted MPD and TMC were removed from membrane surface by rinsing the membrane with hexane. The rinsed membrane was then dried at ambient condition for 1min and in an oven (90^{o}C) for 10 min to complete the reaction between MPD and TMC. A DI water container was used to store the fabricated membrane before testing. Based on the quantity of the used HNTs, the prepared composite membranes are labeled as TFC (control), TFN0.01, TFN0.05 and TFN0.1, respectively.

2.3. Evaluation of membrane performance

The filtration experiments were performed in a self-stirred membrane permeation cell made of stainless-steel material (HP4750, STERLITECH TM). During the process, agitation was provided at the constant speed of 350 rpm to minimize the effect of concentration polarization. Aqueous 2000 ppm NaCl solution was used as feed solution and experiments were carried out at 15 bar gauge and ambient temperature. The following equation was used to determine pure water flux (*J*) of the fabricated membranes [30].

$$J = \frac{\Delta V}{A_m . \Delta t} \qquad (1)$$

where A_m , ΔV, and Δt refer to effective membrane area (14.6 cm^2), permeate volume (L), and time (h), respectively.

Salt rejection of membrane (R) was calculated using the following equation.

$$R = (1 - \frac{C_p}{C_f}) \times 100 \qquad (2)$$

where C_f and C_p are the salt concentrations (mg/L), determined by conductivity measurement, in the feed and permeate solution, respectively.

2.4. Fouling experiments

Hydrodynamic operating condition and feed water composition are the two main factors that control the fouling characteristics of RO membranes. The feed solution with concentration of 10 mM and 200 mg/L were prepared by adding NaCl and BSA (acted as foulant), respectively in the DI solution. The RO experiment continued for 10 h. In order to determine water flux as a function of time, permeate flux was inscribed every 6 min. The collected permeate was returned to RO permeation cell to remain the feed concentration almost constant. After fouling runs, the BSA fouled membranes surface were rinsed with DI water for 30 min. Eventually, the water flux of rinsed membranes were reported according to the same process as described above.

2.5. HNTs and composite membrane characterization

Characteristics of the functional groups in HNTs and TFN membranes were studied using ATR-FTIR spectroscope (Thermo Nicolet Avatar 360). X-ray diffractometer (D/max-rB 12 kW Rigaku, Japan) was employed to identify the XRD patterns of the TFN membranes at 2θranging from 10^o to 80^o (0.1° step size and 1 second/step). The FESEM surface images of the TFC and TFN membranes were obtained using a tabletop microscope (TM3000, Hitachi, Japan). Atomic force microscope (Seiko SPA-300 HV, Japan) was used to investigate the surface morphology and to obtain mean roughness (R_a) of the TFC and TFN membranes. OCA15plus video-based optical contact angle measuring instrument (DataPhysics instrument, Germany) was utilized to measure the water contact angle (CA) of the membrane surface with distilled water at room temperature. The measurement was performed at various locations on the membrane surface, and the average of the measured values was considered as the CA of the membrane. A streaming current electro kinetic analyser (SurPASS, Anton Paar GmbH, Austria) was used to measure the membrane zeta potential. Values of zeta potential were calculated from the measured streaming potential data using the Fair brother-Mastin method[31]. An electrolyte solution containing 10 mM KCl was used to perform the streaming potential measurements as well as flushing the cell before automatic pH titration. Automatic pH titration was carried out using either hydrochloric acid (0.1 M) or potassium hydroxide (0.1 M). All measurements were carried out at room temperature.

3.Results and discussion

3.1 Characteristics of HNTs

Halloysite ($Al_2Si_2O_5(OH)_4.2H_2O$)which is formed by wrapping of the clay mineral layers around themselves to create hollow cylinders, is usually consisted of multi-walled nanotubular-shaped crystals and open-ended lumens. The nanotubular-shaped structure of HNT can be evidenced from the FESEM images shown in Figure 1 at two different scale bars. Figure 2 represents schematically the crystalline structure of HNTs and structure of a single tubular HNT. The external and internal surfaces of HNTs contain siloxane (Si-O-Si) and aluminol (Al-OH) groups, respectively.

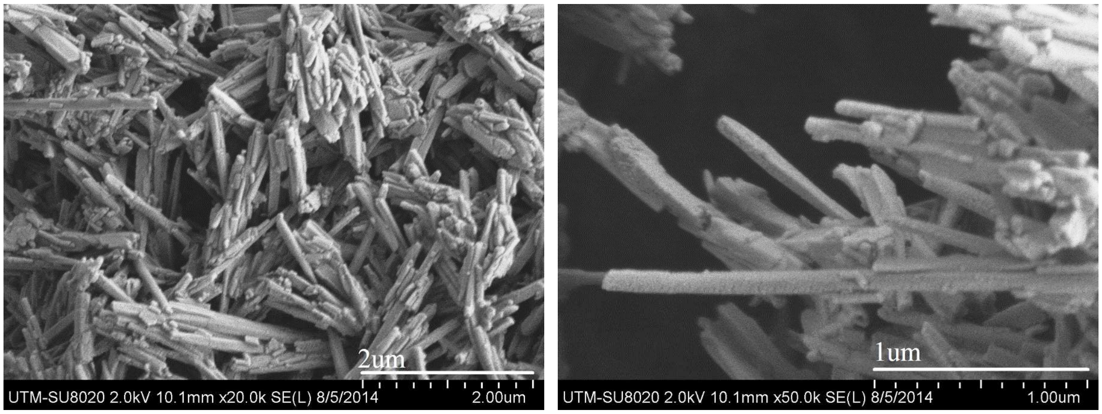

(a) (b)

Fig 1: FESEM images of HNTsat different magnification, (a) 20,000× and (b) 50,000×

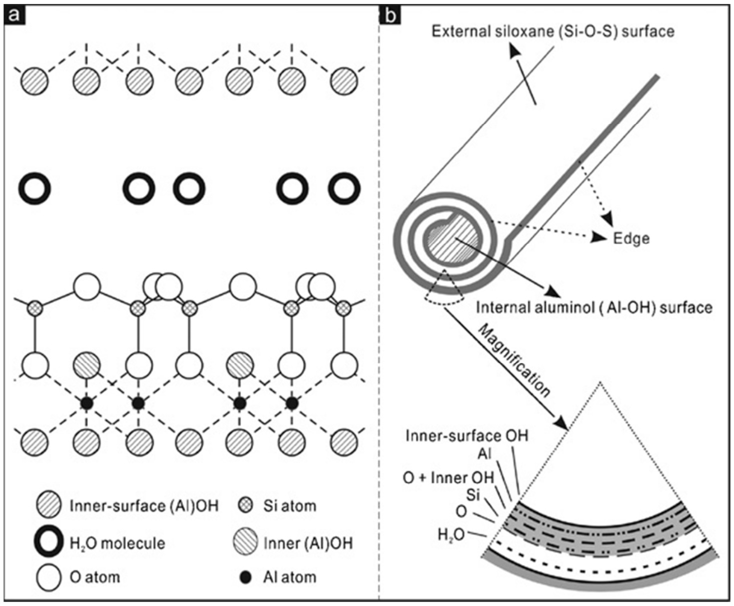

Fig 2: Schematic diagrams of (a) the crystalline structure of halloysite, and (b) the structure of a HNT[32]

3.2 Effect of HNTs loadings on TFN membrane

Molecular bonding and interactions were analysed usingATR-IR technique and the results are presented in Figure 3. The peaks at specific wave numbers of 1149 cm^{-1} (symmetric O=S=O stretching), 1242 cm^{-1} (asymmetric C–O–C stretching), 1292 cm^{-1} (asymmetric O=S=O stretching), 1411 cm^{-1} (C=C aromatic ring stretching) and 1504 cm^{-1} (CH_3–C–CH_3 stretching) represent the specific functional groups of the substrate made of PSf polymer [9]. Successful formation of PA layer on PSf substrate (for both TFC and TFN membrane)can be verified by the two new peaks at ~1544 cm^{-1} and ~1610 cm^{-1} which represent C–N stretching and C=O stretching, respectively [33-35]. Compared with TFC, the spectrum of TFN membrane showed three new bands. The 940 cm^{-1}is the transmittance peak of Si–O while 1030 and 912 cm^{-1}are the asymmetrical stretch vibration peak of Si–O–Si and a single Al–OH bending band, respectively[28, 36]. The existence of these three peaks indicates the successful incorporation of HNTs into the PA layer of composite membrane.

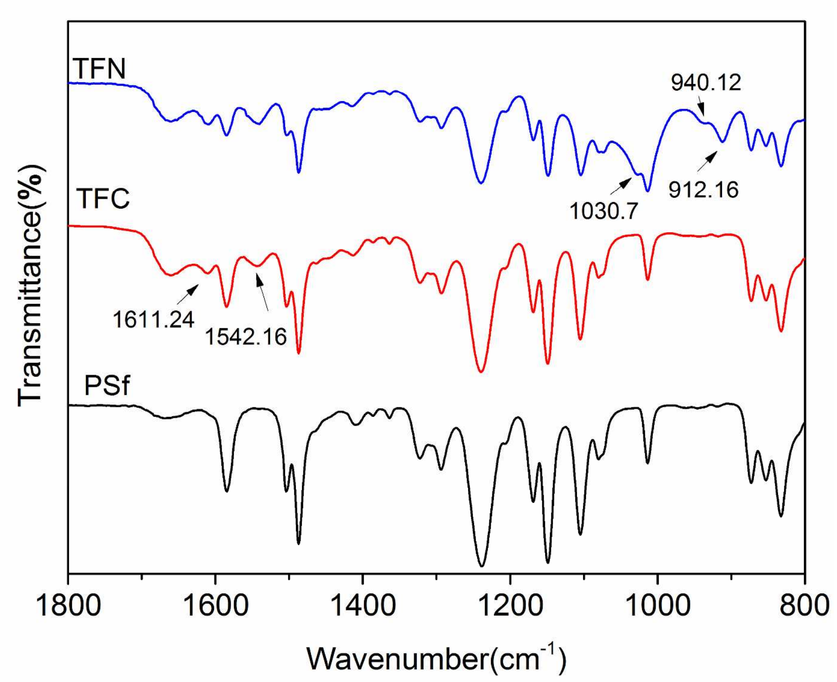

Fig 3: ATR-FTIR spectra from 1900 to 800 cm^{-1}for (a) PSf, (b) TFC membrane and (c) TFN0.1.

The presence of HNTs in the fabricated TFN membranes was further confirmed by XRD (Figure 4) and EDX analysis (Table 1). As can be seen from Figure 4, the XRD patterns of HNTs have two main peaks at $2\theta = 12.2^0$ and $2\theta = 24.6^0$ which refer to $d_{001} = 7.23$Å and $d_{002} = 3.62$ Å, respectively. These patterns are in good agreement with the one previously reported for HNTs [32, 37]. Comparing the HNTs with TFN membrane, it is found that the peak at $2\theta=24.6^0$ shifts to 23.2^0. This is because the in-situ polymerization phenomenon has caused the intercalation of polymer chain into the intralamellar layer of the HNT [38]. Moreover, the absence of HNT peaks in TFC membrane indicates the successful incorporation of HNTs in TFN membrane. The EDX results on the other hand confirmed the existence of HNTs in TFN membranes due to the increasing aluminum and silicon concentration with increasing HNTs quantity. Also, oxygen content increases while carbon and nitrogen decrease progressively with increasing HNTs content, which is another indication of the presence of HNTs at the membrane surface. Figure 5 presents the FESEM images of the top surface and cross-section of the TFC and TFN membranes. At low loading of HNTs, TFN0.01 membrane exhibited the top PA structure very similar to the typical TFC membrane. Nodular surface structure shown by TFC and TFN0.01 membrane is the common morphology for PA films[39]. However, further increase in the HNTs loading to 0.05 wt./v% resulted in more visible "leaf-like" structures in the top surface image and increase in PA layer thickness in the cross-sectional image. Probably, this is the result of the promotion of interfacial polymerization by HNTs[12, 40]. As suggested by Lind et al. [40], the presence of hydrophilic nanomaterials in the organic phase enhances the miscibility of the aqueous and organic phases during interfacial polymerization. Contact between the hydrophilic HNTs in the organic phase and hydrated MPD from the aqueous phase results in particle hydration and release of heat, which accelerate polymerization. With respect to PA layer thickness, it is found that the thickness of PA was obviously reduced with increasing HNTs concentration. It is most likely due to aggregation of HNTs at high HNTs loading. Aggregation can result in poor dispersion of nanomaterials in the PA matrix and decreases the rate of polymerization[2].

Figure 6 compares the top morphological structures of TFC and TFN membranes by 3D AFM images. Based on the AFM images, both TFC and TFN composite membranes exhibited "ridge-and-valley" PA structure. It can be observed that the addition of HNTs in the organic phase of TFN membrane has created higher ridges. Also, as discussed earlier, the TFN membranes developed more obvious 'leaf-like' folds in FESEM images. Therefore, the transparent 'leaf-like' folds in FESEM images can be translated into the observed high ridges in the AFM images. Table 2 summarizes the recorded values of R_a, R_{ms}, and R_{pv} in nanoscopic scale. Obviously, increase in HNTs loading enhances the values of all three variables. The reason is due to the enhanced diffusion of diamine towards the IP zone that is caused by the affinity of the MPD aqueous solution towards the hydrophilic nanotubes. The diffusion rate of diamine into organic solution of acid chlorides is increased by the unstable flow towards nanotubes in the hexane phase. As a result, distribution of the reaction sites changes when the amide linkage is formed. Consequently, varying thicknesses with higher peaks and lower valleys are created[12].

As presented in Figure 7,the contact angle of TFN membranes decreased from 73.1±2.7° to 52.9±1.4° with increasing HNTs loading from 0 to 0.1 wt/v%. This is due to the hydrophilic property of HNTs, which enhances membrane hydrophilicity upon their incorporation into PA layer. Membrane water flux can also be improved due to the capability of the hydrophilic pores of HNTs to draw water via capillary effects [41].

It has been previously reported that performances of PA composite membrane such water permeability and salt separation as well as interactions between the membrane and the foulants in the liquid feed are largely influenced by electrochemical characteristics of the membrane top PA selective layer[42]. The pH-dependent zeta potential of both control TFC and TFN0.05 membranes, measured over the pH range of 4–9, is presented in Figure 8.It was observed that TFN0.5 exhibited more negative zeta potential compared to the control TFC membrane. As shown by Qi et al.,[43] the surface of HNTs is highly negatively charged (−16 to −48 mV) over a wide pH range of 1.5–12.5. Therefore, the incorporation of HNTs nanoparticles can exert additional negative charge on the surface of TFN membrane prepared.

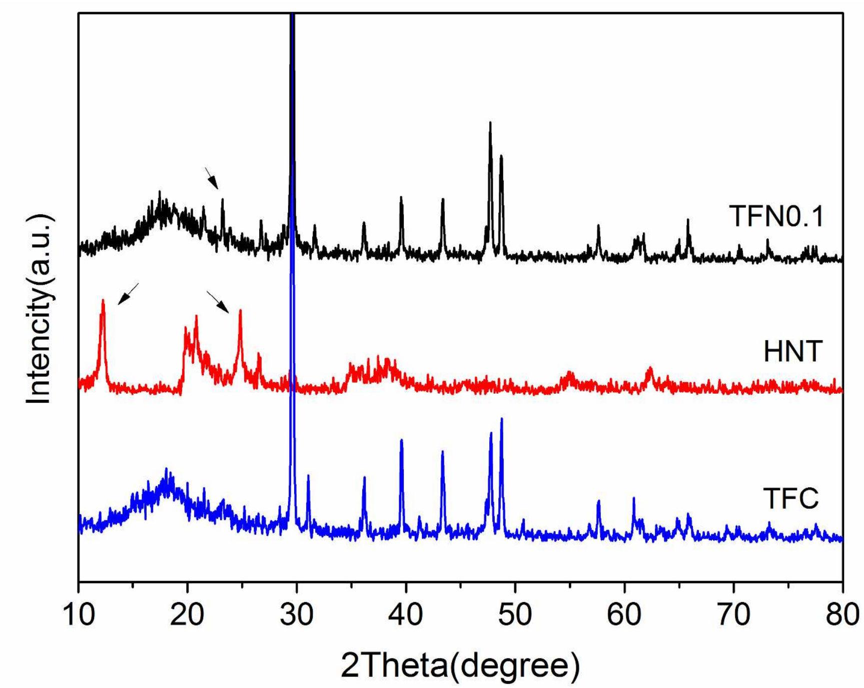

Fig 4:Comparison between XRD patterns of HNTs and composite membranes prepared.

Table 1. EDX results on the topsurface of TFC and TFN membrane

Membrane			Element (wt%)			Total (wt%)
	Carbon	Oxygen	Nitrogen	Aluminum	Silicon	
TFC	67.31	21.43	11.26	-	-	100
TFN0.01	56.59	26.28	15.52	0.84	0.79	100
TFN0.05	48.43	33.36	9.89	4.49	3.83	100
TFN0.1	44.50	36.74	8.01	5.76	4.98	100

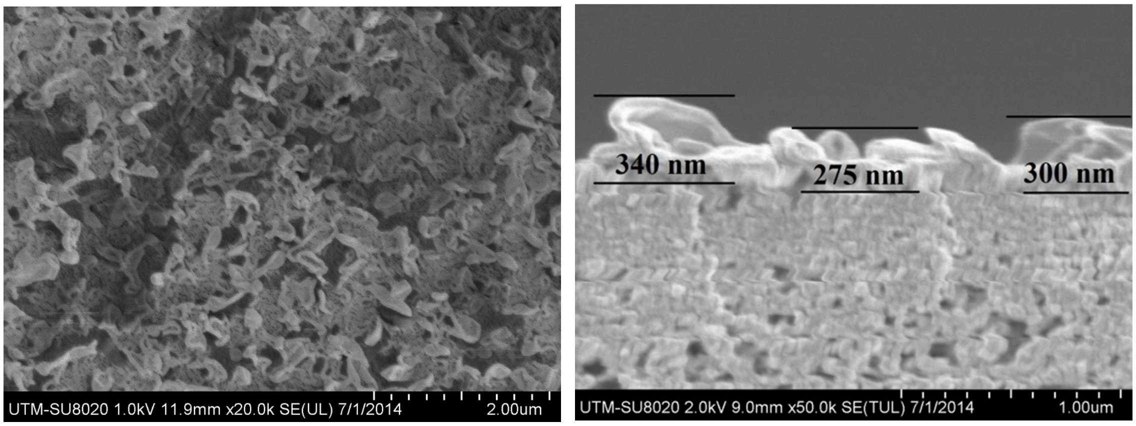
340 nm
275 nm
300 nm
UTM-SU8020 1.0kV 11.9mm x20.0k SE(UL) 7/1/2014 2.00um
UTM-SU8020 2.0kV 9.0mm x50.0k SE(TUL) 7/1/2014 1.00um

(a)

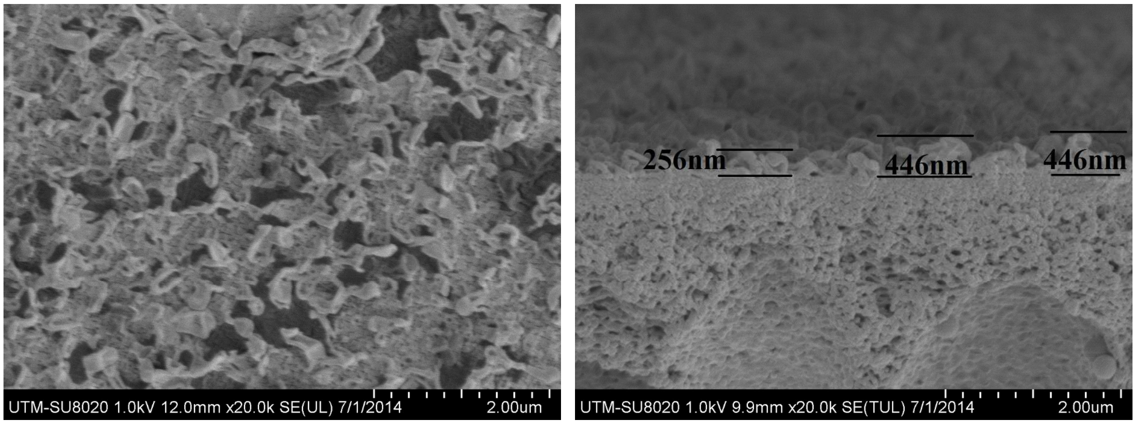
256nm
446nm
446nm
UTM-SU8020 1.0kV 12.0mm x20.0k SE(UL) 7/1/2014 2.00um
UTM-SU8020 1.0kV 9.9mm x20.0k SE(TUL) 7/1/2014 2.00um

(b)

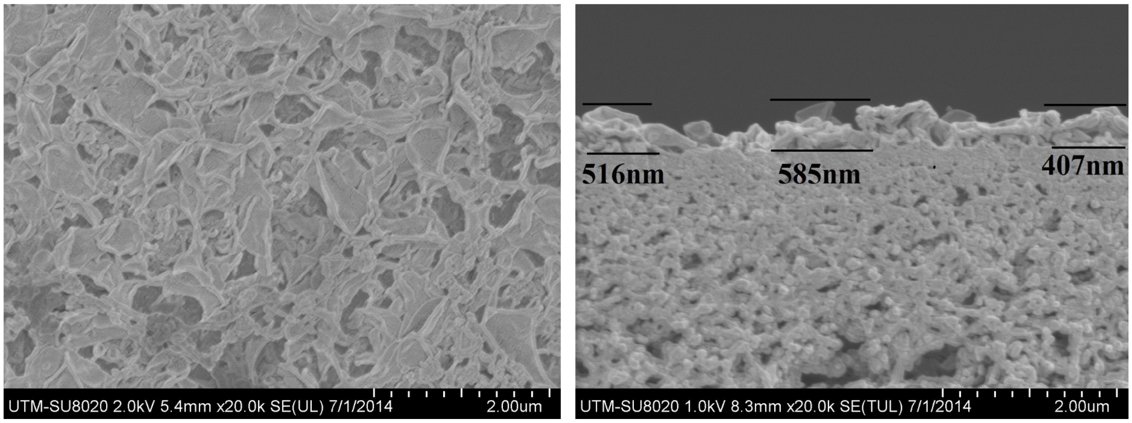
516nm
585nm
407nm
UTM-SU8020 2.0kV 5.4mm x20.0k SE(UL) 7/1/2014 2.00um
UTM-SU8020 1.0kV 8.3mm x20.0k SE(TUL) 7/1/2014 2.00um

(c)

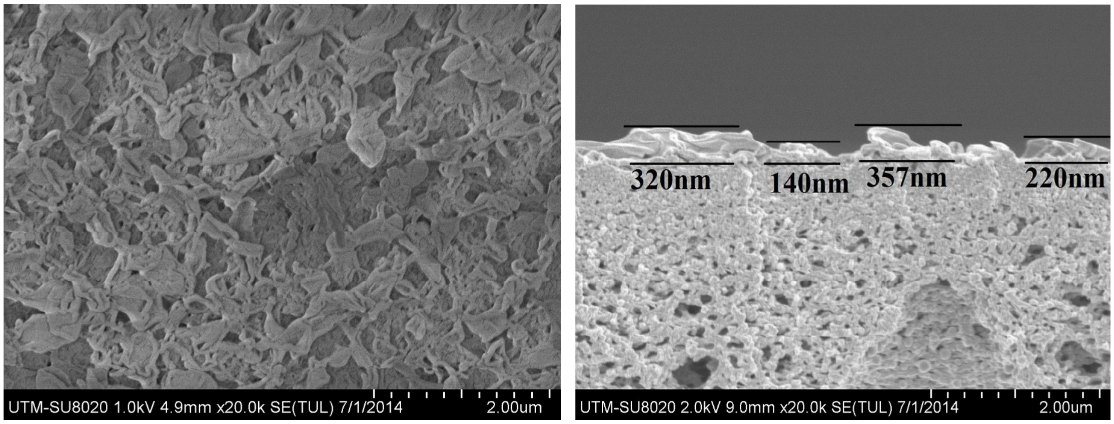

(d)

Fig 5: FESEM images of the top surface and cross section of TFN prepared from different HNT loadings, (a) TFC, (b) TFN0.01, (c) TFN0.05 and (d) TFN0.1

Table 2.Root average arithmetic roughness (R_a) and root mean surface roughness (R_{ms}) and root peak-to-valley (R_{pv})values of the TFC and TFN membranes.

Membrane	R_a (nm)	R_{ms}(nm)	R_{pv} (nm)
TFC	41.5	51.8	188.3
TFN0.01	54.0	65.7	308.5
TFN0.05	61.4	76.4	365.2
TFN0.1	75.7	94.1	373.7

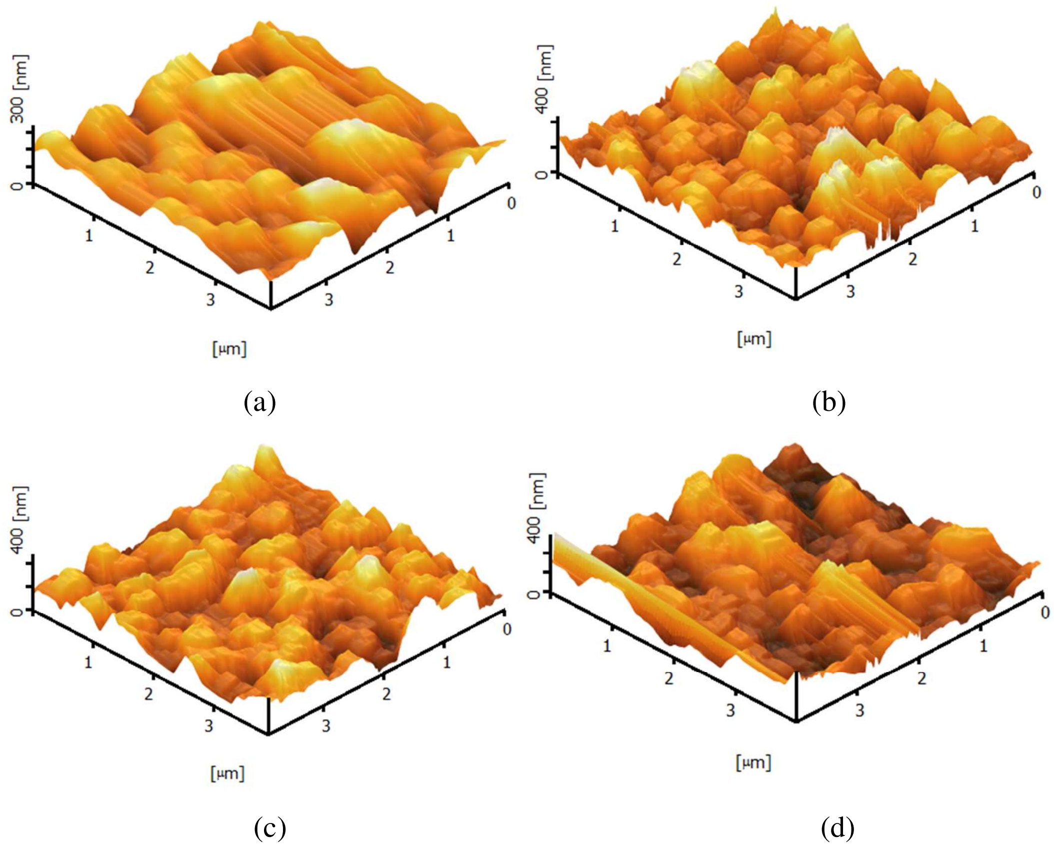

(a) (b)

(c) (d)

Fig 6: 3D AFM images of the top surface of (a) TFC, (b) TFN0.01, (c) TFN0.05 and (d) TFN0.1

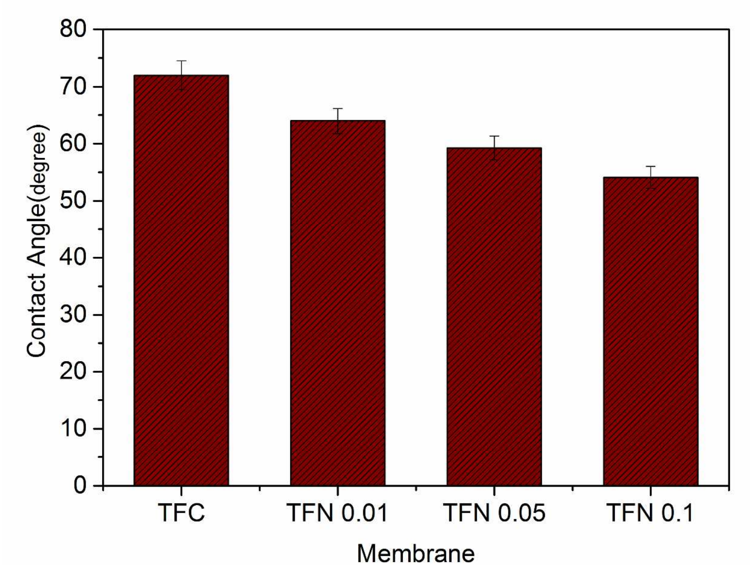

Fig 7:Water contact angle of TFN membranes.

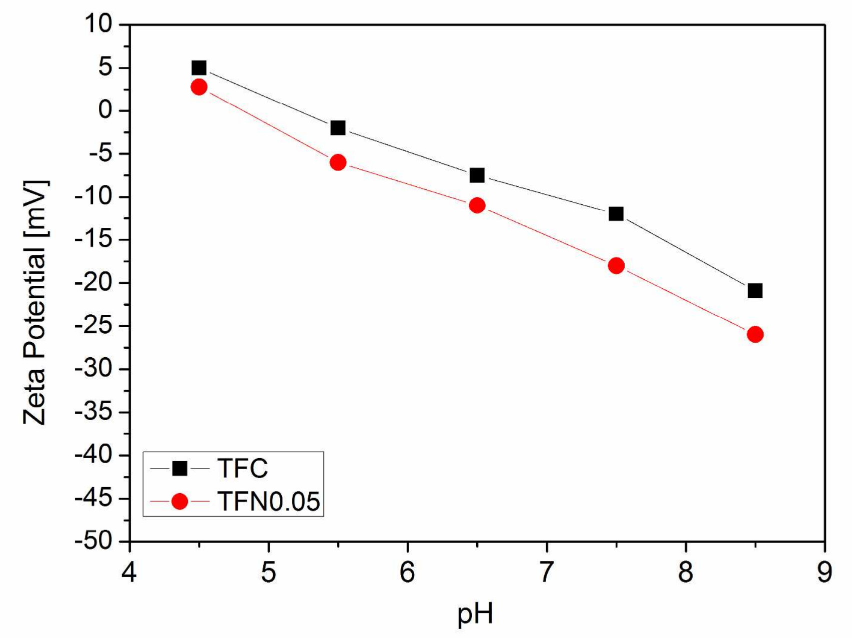

Fig 8: Zeta potential of TFC and TFN0.05 membrane

3.3 Effect of HNTs loading on the performance of TFN membrane during RO experiments

Figure 9shows the effect of HNTs loading on the separation characteristics of the composite membraneswith respect to water flux and salt rejection. As shown, the flux increased progressively from 19 L/m^{2}h of TFC membrane to 48 L/m^{2}h of TFN0.1 membrane. This enhancement of water flux can be explained by considering the following three water channels.

1) Increase in the area of PA surface that is in contact with the feed solution due to the formation of leaf-like structure.
2) Formation of voids formed at the inter face between embedded HNTs and polymer creates water flow channels in addition to the diffusion through the PA matrix.
3) Presence of the internal pores of HNTs that provide short flow paths for water molecules, facilitating the water permeability of membranes.

In addition, the improved membrane surface hydrophilicity upon HNTs incorporation could also improve solubilization and diffusion of water molecules to certain extent into the membrane [41, 44].

In terms of separation efficiency, it is found that the salt rejection decreased progressively with increasing HNTs loading; i.e. it decreased from 97.2%TFCto 80.5% of TFN0.1 membrane. Among the three channels mentioned above,

1) Salt rejection by the PA matrix does not change.

2) Salt rejection by the void space between HNTs and PA matrix is low because of the large channel size.
3) As well, the salt rejection by the internal pores of HNTs is low considering the large diameter of the pores, despite the electrical charges HNTs (positive at the internal surface and negative at the external surface[20]).

Thus, formation of new permeation channels 2)[45] and 3) seems the main reason for the reduction of salt rejection.

A remarkable decrease in salt rejection is observed from TFN 0.05 to TFN0.1, which is due to HNTs aggregation at high concentration. Large pores are formed between the aggregated HNTs particles, leading to further reduction of salt rejection. This explanation can be further supported by the information obtained from FESEM image of TFN0.1. While maintaining high salt rejection, TFN0.05 was able to provide 90% more water flux compared to the original TFC. Therefore, TNF0.05 was selected for further organic fouling evaluation.

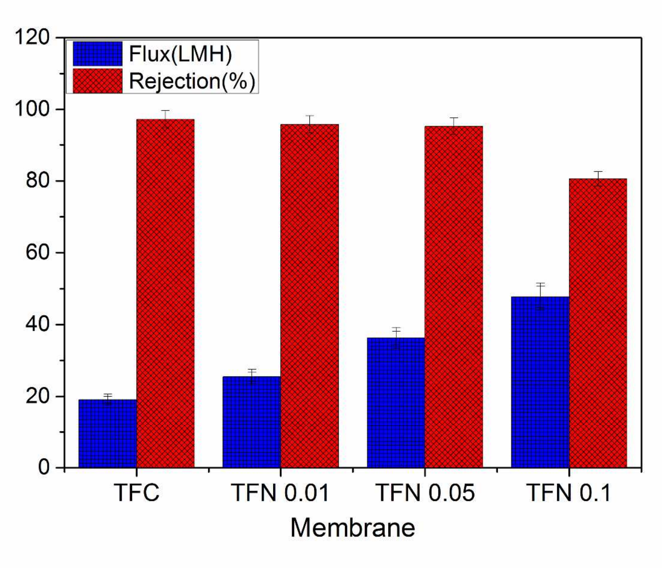

Fig 9: Water flux and NaCl rejection of TFC and TFN membranes (Test conditions: 15 bar and 2000 ppm salt solution)

Table 3. Summary of the properties and performances of TFN membranes for water desalination

Membranes (PA layer thickness)	Filler type	Optimized membrane	Operation pressure (bar)	Water flux $(L/m^2.h)$	Salt rejection (%)	Reference
HNTs–polyamide (200–500 nm)	HNTs (ID:5nm–15 nm)	TFN0.05	15	36.1	95.6	In this work
CNTs–polyamide (100–300 nm)	CNTs (ID:5nm)	TFN0.1	16	28.05	90	17
Silica-polyamide (300–500 nm)	Silica (MCM-41) nanoparticles (100 nm)	TFN0.1	20	46.6	97.9	41
NaX–polyamide (200–300 nm)	Zeolite (NaX) nanocrystals (40 nm–150 nm)	TFN0.2	12	29.76	96.4	46
Aluminosilicate – polyamide (100–400 nm)	Aluminosilicate nanotubes (ID: 1nm)	TFN0.2	16	27.3	95.4	12
Zeolite A–polyamide (50–200 nm)	Zeolite A nanocrystals (50 nm–150nm)	TFN0.4	12	16.96	93.9	44

3.4 Effects of HNTs on the organic fouling behavior of TFN membrane

The fluxes of TFC and TFN0.05 membranes are shown as a function of operation period in Figure 10, when the feed solution contains BSA. As can be seen, the flux of TFN0.05 decreases more slowly than TFC. As shown by Qi et al.,[43] the surface of HNTs is highly negatively charged (-16 to -48 mV over a pH range of 1.5-12.5) in a wide range of pH. Hence, the electrostatic repulsion working negatively charged BSA molecules and the HNTs incorporated membrane surface seems the major contribution to the reduction of membrane fouling by BSA [47]. High hydrophilicity of membrane surface due to incorporation of HNTs can be considered as another factor in preventing protein adsorption at the surface of the TFN membrane [48].The normalized flux of both membranes before and after cleaning process was compared and results are presented in Figure 11. While TFC membrane reached 69% water recovery after 30 min of water rinsing, TFN0.05 membrane exhibited superior performance by obtaining 91% water recovery under the same conditions. Excellent foulant removal of the TFN membranes in this study can be, once again, linked to the improved hydrophilicity of the membrane surface which weakened the interactions between PA dense layer and the foulant.

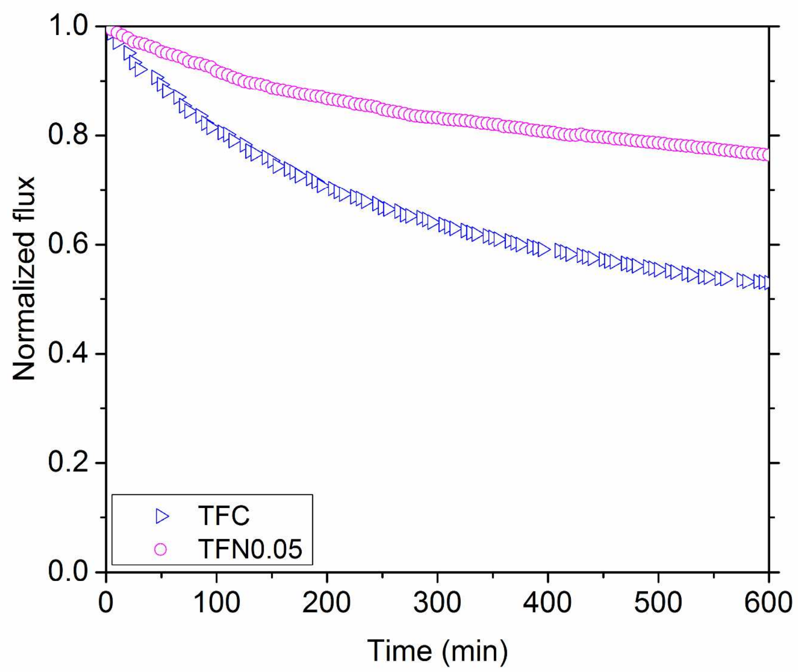

Fig10: The effect of HNTs on the organic fouling of RO membrane

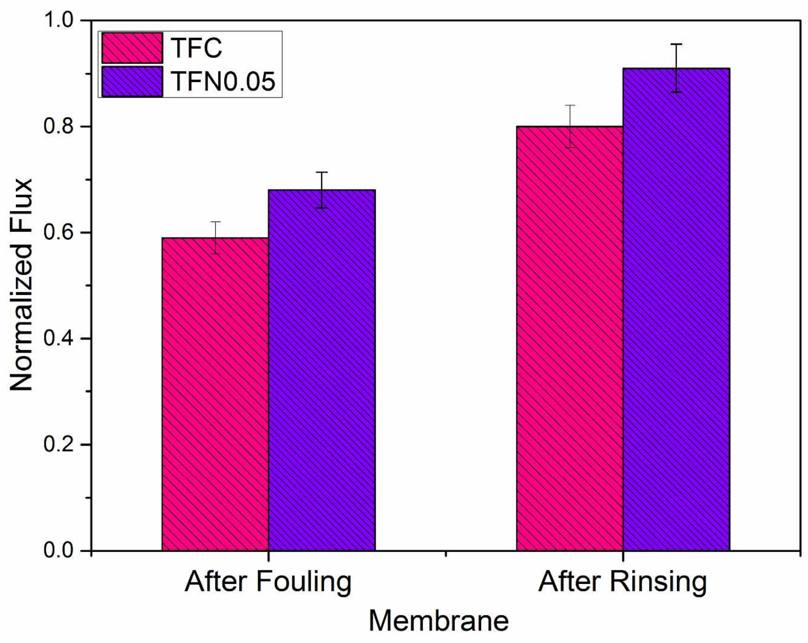

Fig 11. Normalized water fluxes of the BSA-fouled raw TFC and TFN0.05 membrane before and after washing with DI water.

4. Conclusions

In this work, hydrophilic HNTs were incorporated in the top surface layer of a TFC membrane during an in-situ interfacial polymerization of MPD and TMC to produce TFN membrane. The prepared membrane was characterized and tested for RO applications and the following conclusions were made. XRD and FTIR analysis verified the presence of HNTs in the TFN membranes while EDX confirmed the increasing quantities of HNTs in the PA layer with increasing HNTs loadings. Hydrophilicity and roughness of the TFN membranes increased with an increase in HNTs loading. The "leaf-like" outgrowth morphology of PA layer was observed by FESEM in the membranes made of high HNTs loading. It is most probably due to promotion of interfacial polymerization by HNTs. The transparent 'leaf-like' folds in FESEM images can be translated into the high ridges observed in the AFM images. The introduction of HNTs in to PAactive layer of composite membranes improved the RO water flux significantly. This water flux enhancement can be due to higher hydrophilicity and formation of additional water pathways through porous HNTs in TFN membranes.The water flux of membrane was significantly increased from 19 L/m^2.hr of TFC (control) to 36 L/m^2.hr of TFN0.05, withonly slight decrease in NaCl separation from 97.2% to 95.6%. The antifouling capacity of TFN0.05 in the presence of BSA in the feed was compared with control TFC membrane.The flux decline of TFN0.05 membrane was slower than TFC membrane, indicating the enhancement of fouling resistance by incorporation of HNTs, which could be attributed to higher hydrophilicity as well as the negative charge of TFN0.05 membrane.

References

1. M. Bao, G. Zhu, L. Wang, M. Wang and C. Gao, *Desalination*, 2013, 309, 261-266.
2. H. Huang, X. Qu, X. Ji, X. Gao, L. Zhang, H. Chen and L. Hou, *Journal of Materials Chemistry A*, 2013, 1, 11343-11349.
3. D. Emadzadeh, W. J. Lau and A. F. Ismail, *Desalination*, 2013, 330, 90-99.
4. D. Emadzadeh, W. J. Lau, T. Matsuura, A. Ismail and M. Rahbari-Sisakht, *Journal of Membrane Science*, 2014, 449, 74-85.
5. W. J. Lau, A. Ismail, P. Goh, N. Hilal and B. Ooi, *Separation & Purification Reviews*, 2015, 44, 135-156.
6. T. Shintani, H. Matsuyama and N. Kurata, *Desalination*, 2009, 247, 370-377.
7. A. K. Ghosh, B.-H. Jeong, X. Huang and E. Hoek, *Journal of Membrane Science*, 2008, 311, 34-45.
8. G. Kang, M. Liu, B. Lin, Y. Cao and Q. Yuan, *Polymer*, 2007, 48, 1165-1170.
9. B. J. A. Tarboush, D. Rana, T. Matsuura, H. Arafat and R. Narbaitz, *Journal of Membrane Science*, 2008, 325, 166-175.
10. Y.-H. La, R. Sooriyakumaran, D. C. Miller, M. Fujiwara, Y. Terui, K. Yamanaka, B. D. McCloskey, B. D. Freeman and R. D. Allen, *Journal of Materials Chemistry*, 2010, 20, 4615-4620.
11. S. Yu, Q. Zhou, S. Shuai, G. Yao, M. Ma and C. Gao, *Desalination*, 2013, 315, 164-172.
12. G. N. B. Baroña, J. Lim, M. Choi and B. Jung, *Desalination*, 2013, 325, 138-147.

13. D. Li and H. Wang, *Journal of Materials Chemistry*, 2010, 20, 4551-4566.
14. J. Mansouri, S. Harrisson and V. Chen, *Journal of Materials Chemistry*, 2010, 20, 4567-4586.
15. R.-X. Zhang, L. Braeken, P. Luis, X.-L. Wang and B. Van der Bruggen, *Journal of Membrane Science*, 2013, 437, 179-188.
16. H. J. Kim, Y. Baek, K. Choi, D.-G. Kim, H. Kang, Y.-S. Choi, J. Yoon and J.-C. Lee, *RSC Advances*, 2014, 4, 32802-32810.
17. H. Zhao, S. Qiu, L. Wu, L. Zhang, H. Chen and C. Gao, *Journal of Membrane Science*, 2014, 450, 249-256.
18. A. Tiraferri, C. D. Vecitis and M. Elimelech, *ACS applied materials & interfaces*, 2011, 3, 2869-2877.
19. J. Zhang, Y. Zhang, Y. Chen, L. Du, B. Zhang, H. Zhang, J. Liu and K. Wang, *Industrial & Engineering Chemistry Research*, 2012, 51, 3081-3090.
20. Y. Joo, Y. Jeon, S. U. Lee, J. H. Sim, J. Ryu, S. Lee, H. Lee and D. Sohn, *The Journal of Physical Chemistry C*, 2012, 116, 18230-18235.
21. H. Chen, J. Zhao, J. Wu and H. Yan, *RSC Advances*, 2014, 4, 15389-15393.
22. Y. Liu, X. Jiang, B. Li, X. Zhang, T. Liu, X. Yan, J. Ding, Q. Cai and J. Zhang, *Journal of Materials Chemistry A*, 2014, 2, 4264-4269.
23. H. Ismail, P. Pasbakhsh, M. Fauzi and A. Abu Bakar, *Polymer Testing*, 2008, 27, 841-850.
24. Y. Chen, Y. Zhang, H. Zhang, J. Liu and C. Song, *Chemical Engineering Journal*, 2013, 228, 12-20.
25. C. Liu, L. Yu, Y. Zhang, B. Zhang, J. Liu and H. Zhang, *RSC Advances*, 2013, 3, 13756-13763.
26. C. Li, J. Wang, S. Feng, Z. Yang and S. Ding, *Journal of Materials Chemistry A*, 2013, 1, 8045-8054.
27. X. Ding, H. Wang, W. Chen, J. Liu and Y. Zhang, *RSC Advances*, 2014, 4, 41993-41996.
28. H. Yu, Y. Zhang, X. Sun, J. Liu and H. Zhang, *Chemical Engineering Journal*, 2014, 237, 322-328.
29. Y. Chen, Y. Zhang, J. Liu, H. Zhang and K. Wang, *Chemical Engineering Journal*, 2012, 210, 298-308.
30. D. Emadzadeh, W. J. Lau, T. Matsuura, M. Rahbari-Sisakht and A. Ismail, *Chemical Engineering Journal*, 2014, 237, 70-80.
31. M. Elimelech, W. H. Chen and J. J. Waypa, *Desalination*, 1994, 95, 269-286.
32. P. Yuan, P. D. Southon, Z. Liu, M. E. Green, J. M. Hook, S. J. Antill and C. J. Kepert, *The Journal of Physical Chemistry C*, 2008, 112, 15742-15751.
33. N.-N. Bui, M. L. Lind, E. Hoek and J. R. McCutcheon, *Journal of Membrane Science*, 2011, 385, 10-19.
34. P. S. Singh, S. Joshi, J. Trivedi, C. Devmurari, A. P. Rao and P. Ghosh, *Journal of membrane science*, 2006, 278, 19-25.
35. X. Wei, X. Kong, C. Sun and J. Chen, *Chemical Engineering Journal*, 2013, 223, 172-182.
36. M. L. Lind, D. Eumine Suk, T.-V. Nguyen and E. M. Hoek, *Environmental science & technology*, 2010, 44, 8230-8235.
37. A. F. Ismail, S. Hashemifard and T. Matsuura, *Journal of Membrane Science*, 2011, 379, 378-385.
38. R. Surya Murali, M. Padaki, T. Matsuura, M. Abdullah and A. Ismail, *Separation and Purification Technology*, 2014.
39. A. K. Ghosh and E. Hoek, *Journal of Membrane Science*, 2009, 336, 140-148.
40. M. L. Lind, A. K. Ghosh, A. Jawor, X. Huang, W. Hou, Y. Yang and E. M. Hoek, *Langmuir*, 2009, 25, 10139-10145.
41. J. Yin, E.-S. Kim, J. Yang and B. Deng, *Journal of Membrane Science*, 2012, 423, 238-246.
42. T. Chiu and A. James, *Colloids and Surfaces A: Physicochemical and Engineering Aspects*, 2007, 301, 281-288.
43. R. Qi, R. Guo, M. Shen, X. Cao, L. Zhang, J. Xu, J. Yu and X. Shi, *Journal of Materials Chemistry*, 2010, 20, 10622-10629.

44. B.-H. Jeong, E. Hoek, Y. Yan, A. Subramani, X. Huang, G. Hurwitz, A. K. Ghosh and A. Jawor, *Journal of Membrane Science*, 2007, 294, 1-7.
45. H. Wu, B. Tang and P. Wu, *Journal of Membrane Science*, 2013, 428, 341-348.
46. M. Fathizadeh, A. Aroujalian and A. Raisi, *Journal of membrane science*, 2011, 375, 88-95.
47. S. Boributh, A. Chanachai and R. Jiraratananon, *Journal of Membrane Science*, 2009, 342, 97-104.
48. D. Emadzadeh, W. J. Lau, T. Matsuura, N. Hilal and A. Ismail, *Desalination*, 2014, 348, 82-88.

List of Figure

List of Table